Journal of Crystal Growth 546 (2020) 125738

Contents lists available at ScienceDirect

Journal of Crystal Growth

journal homepage: www.elsevier.com/locate/jcrysgro

# High nitrogen flux plasma-assisted molecular beam epitaxy growth of $In_xGa_{1-x}N$ films

Kelsey F. Jorgensen*, Bastien Bonef, James S. Speck

*Materials Department, University of California, Santa Barbara, CA 93106, United States*

ARTICLE INFO

Communicated by H. Asahi

*Keywords:*
A1. Atomic Force Microscopy
A1. Atom Probe Tomography
A1. High Resolution X-Ray Diffraction
A3. Molecular Beam Epitaxy
B1. Nitrides

ABSTRACT

Growth of efficient III-N based light emitting devices by plasma assisted molecular beam epitaxy has been elusive, even though the technique has attractive advantages in comparison to metal organic chemical vapor deposition. Modern high-flux radio frequency plasma systems could remedy this issue by enabling growth of $In_xGa_{1-x}N$ at higher temperatures than previously possible, likely improving the material quality. In this work, active nitrogen fluxes of up to 3.5 μm/h GaN-equivalent growth rate were employed to grow $In_xGa_{1-x}N$ alloys. $In_xGa_{1-x}N$ growth rates of 1.3 μm/h were demonstrated at growth temperatures of 550 °C and 600 °C with maximum film compositions of $In_{0.25}Ga_{0.75}N$ and $In_{0.21}Ga_{0.79}N$, respectively. A composition of $In_{0.05}Ga_{0.95}N$ was observed in a film grown at 700 °C with smooth step-terrace morphology.

## 1. Introduction

III-N multi-quantum well (MQW) light-emitting diodes (LEDs) with $In_xGa_{1-x}N$ active regions have enabled energy-efficient white lighting sources. While all commercial devices today are grown by metal organic chemical vapor deposition (MOCVD), plasma-assisted molecular beam epitaxy (PAMBE) offers a unique opportunity to grow $In_xGa_{1-x}N$ with higher In-content than $NH_3$-based growth methods. Unlike MOCVD and $NH_3$-Assisted MBE, PAMBE does not rely on the thermal decomposition of $NH_3$ to supply nitrogen to the growth surface. This enables growth at lower temperatures, and thus higher In content $In_xGa_{1-x}N$, and even high-quality pure InN, is readily achievable.

The drawback of lower temperature growth, however, is a decrease in adatom mobility on the film surface, making smooth morphologies difficult to achieve. To overcome this, $In_xGa_{1-x}N$ is typically grown under a highly-mobile saturated 2.5 monolayer In adlayer that acts a surfactant by increasing the adatom mobility [1]. The adlayer presence also has the added benefit of creating a nearly constant alloy composition at a given temperature. PAMBE also enjoys low background impurity concentration as well as active as-grown p-GaN. This enables p-GaN to be placed anywhere in an epi-structure, enabling device designs that are unavailable to MOCVD due to the challenges of activating the Mg acceptors for buried GaN:Mg layers. Despite the advantages of PAMBE growth, attempts at an all-PAMBE nitride LEDs have been few, and published efficiency values have been poor [2–4].

Regardless of technique, the growth of $In_xGa_{1-x}N$ alloys is challenging due to the large difference in thermal stability of its constituent materials, GaN and InN. In vacuum, In-N bonds begin to decompose at 435 °C [1], whereas Ga-N bonds do not decompose for temperatures lower than ~720 °C [5]. This means that the optimal growth temperature for $In_xGa_{1-x}N$ is very different from that of GaN. For PAMBE, $In_xGa_{1-x}N$ growth typically takes place between 500 °C and 650 °C in a regime where In-N bonds are actively decomposing. The alloy composition is thus extremely temperature dependent. Since the Ga-N bonds are significantly more stable than In-N bonds, the supplied Ga-flux ($\Phi_{Ga}$) to the $In_xGa_{1-x}N$ must be less than the supplied active nitrogen flux ($\Phi_{N^*}$), otherwise no In will incorporate in the growing layer [6]. For $In_xGa_{1-x}N$ growth under a saturated In wetting layer, to very good approximation, the Indium composition x in the $In_xGa_{1-x}N$ film is determined by the growth temperature.

The exact identity of the active nitrogen species that participates in III-N growth from RF plasma units remains a matter of debate. Carefully conducted appearance mass spectroscopy (AMS) experiments have indicated that the species that reaches the substrate is atomic N [7], however optical emission spectroscopy (OES) from the back viewport of the plasma has indicated that a *meta*-stable excited $N_2$ molecule is also present [8,9]. It is beyond the scope of this report to make a determination about the identity of the active species, and for simplicity the active nitrogen will be represented as N*.

Two methods of growing $In_xGa_{1-x}N$/GaN quantum well/quantum barrier (QW/QB) active regions via PAMBE currently exist. In one method, the sample is heated and cooled between layers. $In_xGa_{1-x}N$

* Corresponding author.
*E-mail address:* kelseyjorgensen@ucsb.edu (K.F. Jorgensen).

https://doi.org/10.1016/j.jcrysgro.2020.125738
Received 27 April 2020; Received in revised form 24 May 2020; Accepted 26 May 2020
Available online 11 June 2020

QWs are grown at a low temperature, then a thin, low temperature GaN "cap" is grown on the $In_xGa_{1-x}N$ layer before the sample is heated to suppress subsequent $In_xGa_{1-x}N$ decomposition. Then the remainder of the GaN QB is grown at the higher growth temperature. This way both the QWs and the majority of the QBs are both grown at the optimal $In_xGa_{1-x}N$ and GaN growth temperatures, respectively. These growth interrupts due to heating and cooling cycles make impurities more likely to segregate on the interfaces between layers, which can produce defects that reduce the radiative efficiency. Another method of growing a MQW region consists of growing the entire region at a lower temperature suited to $In_xGa_{1-x}N$ growth, and using two separate Ga-fluxes to modify the composition of the QWs and QBs [10,11]. In this method a constant In-flux ($\Phi_{In}$) and $\Phi_{N^*}$ are supplied to the film while $\Phi_{Ga}$ is modulated between $\Phi_{Ga1} < \Phi_{N^*}$ for the QWs and $\Phi_{Ga2} \geq \Phi_{N^*}$ for the QBs. This method eliminates growth interrupts between layers, but at the cost of growing the GaN QBs at a temperature lower than the ideal GaN growth temperature.

Modern high flux RF plasma sources can supply over an order of magnitude greater active nitrogen flux than previously possible, enabling reported growth rates as high as 7.6 μm/h [12] and 8.4 μm/h [13] while supplying pure $N_2$ to the plasma source. $\Phi_{N^*}$ of this magnitude enables the exploration of growth regimes previously inaccessible to PAMBE III-N growth. For InN and $In_xGa_{1-x}N$ growth, increasing the N overpressure suppresses In-N bond decomposition. Modeling by Turski et al. [6] predicts that supplying an order of magnitude higher absolute $\Phi_{N^*}$ will result in approximately 10% increase the In composition in $In_xGa_{1-x}N$ films. Utilizing this high $\Phi_{N^*}$ could enable growth of $In_xGa_{1-x}N$ at higher temperatures than previously established, potentially improving the material quality and thus enabling efficient PAMBE-grown $In_xGa_{1-x}N$ based light emitters. If $In_xGa_{1-x}N$ growth could be realized at typical GaN growth temperatures, it could be feasible to grow an entire active region of an LED without growth interrupts at the growth temperature similar to that used for the highest quality PAMBE GaN grown under a saturated Ga adlayer (typically close to 720 °C).

In this work we show the effect of high active nitrogen flux on the incorporation of In into $In_xGa_{1-x}N$ films, and how that higher flux can enable $In_xGa_{1-x}N$ growth at temperatures higher than previously demonstrated for PAMBE. The effect of the high active nitrogen flux on surface morphology is also discussed.

## 2. Experimental methods

All samples were grown in a Varian GenII MBE equipped with two Ga Titan cells (E-Science, Hudson, WI), an In SUMO cell (Veeco, St. Paul, MN), and a modified Riber RFM50/63 RF-plasma source using nitrogen gas (99.9995% purity). The system is equipped with a reflection high energy electron diffraction (RHEED) gun for in-situ monitoring of the crystal surface. During growth, the main chamber is pumped by two cryogenic pumps and an additional ion pump is used when the system is idle. The base pressure of the main chamber is around $1 \times 10^{-10}$ Torr and typical pressures during growth are in the $10^{-5}$ Torr range, depending on the $N_2$ gas flow rate.

The substrate used is a single-side polished GaN:Si on sapphire template from Lumilog St. Gobain. The back of the wafers were coated in 500 nm of Ti to improve thermal contact and to provide a black body source for the optical pyrometer to measure growth temperature. The optical pyrometer emissivity was calibrated to the melting point of Al. The template wafers were diced into $1 \times 1$ cm$^2$ pieces. The cleaning procedure for each sample was 3 min each in acetone, methanol, and isopropanol in an ultrasonic bath. Each wafer piece was then In-bonded to a lapped Si wafer and loaded into the MBE system. Each sample was outgassed for 1 h at 400 °C in vacuum before being loaded into the growth chamber.

To quantify $\Phi_{N^*}$ in terms of a GaN equivalent growth rate, a sample structure of a GaN buffer, 5 nm AlGaN layer, followed by a 100–250 nm Ga-rich GaN layer was grown for each plasma condition. This structure was grown at 720 °C, where Ga-N bond decomposition is negligible. The thickness of the top GaN layer was then determined by measuring the thickness fringes on a high-resolution X-ray diffraction (HRXRD) ω-2θ (0002) scan. The growth thickness was then divided by the growth time to determine the growth rate. To quantify $\Phi_{Ga}$ in terms of a GaN equivalent growth rate the same structure was grown, but this time with an N-rich top GaN layer. The thickness and growth rate were determined in the same manner. This was done for a series of $\Phi_{Ga}$. A plot of growth rate vs. Ga beam equivalent pressure (BEP) was made, and a linear relationship was fitted.

To quantify $\Phi_{In}$ in terms of an InN equivalent growth rate a series of pure InN films were grown on the GaN:Si on sapphire templates at 420 °C where In-N bond decomposition is negligible. The growth was N-rich and $\Phi_{In}$ was varied for each sample. These films were relaxed and rough (as expected), so thickness determination via HRXRD was not possible. Instead the samples were cleaved and the thickness was measured via scanning electron microscopy (SEM) in cross section. As for the $\Phi_{Ga}$ determination, a linear relationship between InN growth rate and In BEP was fitted to the data.

Fluxes given in equivalent growth rates can also be converted into atomic fluxes. One monolayer (ML) of GaN corresponds to $\frac{c_{0,GaN}}{2} = 0.259nm$ with $1.14 \times 10^{15}$ atom/cm$^2$ planar density. In this work atomic fluxes are shown in parentheses beside their equivalent growth rate counterparts. One small issue of this method is that during $In_xGa_{1-x}N$ growth the c lattice spacing differs depending on the film composition $x$. However, since $c_{0/GaN}$ and $c_{0,InN}$ differ by approximately 10%, and the films in this study are all of lower composition ($x \leq 0.25$), using $c_{0,GaN}$ as an approximation of 1 ML will introduce only a small error.

Fig. 1(a) shows the schematic for sample growth. For each sample a GaN buffer layer was first grown at 720 °C under standard Ga-rich conditions using the modulated growth technique [14]. The $N_2$ flow rate was 3 sccm and the plasma forward power was 200 W. This corresponded to a growth rate of about 0.4 μm/h ($4.9 \times 10^{14}$ atom/cm$^2$s). A $\Phi_{Ga}$ of around $8 \times 10^{-7}$ Torr beam equivalent pressure (BEP) was used, which corresponded to about 0.7 μm/h ($8.6 \times 10^{14}$ atom/cm$^2$s). The sample was rotated during buffer growth at 1 rotation per minute (RPM) to ensure that a uniform thickness was deposited over the area of the sample.

After the GaN buffer growth, the temperature was decreased to the desired $In_xGa_{1-x}N$ growth temperature. Next, a coherent $In_xGa_{1-x}N$ layer was grown. The thickness of the $In_xGa_{1-x}N$ layers varied between 20 and 65 nm to ensure that all films were coherent. To initiate $In_xGa_{1-x}N$ growth the In shutter was opened first, and the RHEED intensity transient was monitored. When the RHEED intensity reached a minimum the Ga and N* shutters were opened. After the target growth time is reached, all shutters were simultaneously closed and the adlayer was desorbed. Fig. 1(b) shows the RHEED intensity transient and shutter timing for 30 s of $In_xGa_{1-x}N$ film growth.

The first grown series (Series 1) was grown with a $N_2$ flow rate of 6 sccm and a plasma forward power of 450 W, which corresponded to a N-limited GaN equivalent growth rate of 1.5 μm/h ($1.8 \times 10^{15}$ atom/cm$^2$s). $\Phi_{Ga} = 8 \times 10^{-7}$ Torr BEP was used, which corresponded to a Ga-limited GaN equivalent growth rate of 1.0 μm/h ($1.22 \times 10^{15}$ atom/cm$^2$s). $\Phi_{In}$ was varied from 1 to $8 \times 10^{-7}$ Torr BEP which corresponded to 0.3–1.1 μm/h ($3.7 - 13 \times 10^{14}$ atom/cm$^2$s) InN equivalent growth rate. $In_xGa_{1-x}N$ growth temperatures investigated for Series 1 were 550 °C and 600 °C. Seven samples were grown at 550 °C and seven were grown at 600 °C.

The second grown series (Series 2) was grown with an increased $\Phi_{N^*}$-$\Phi_{Ga}$ deficit to determine how much In incorporation could be achieved at 650 °C and 700 °C. Table 1 lists the fluxes used for the samples in Series 2. To achieve $\Phi_{N^*} = 2.6$ μm/h ($3.2 \times 10^{15}$ atom/cm$^2$s) for samples A2 and B2, a $N_2$ flow of 10 sccm and a plasma forward power of 500 W were used. To achieve 3.5 μm/h N* flow

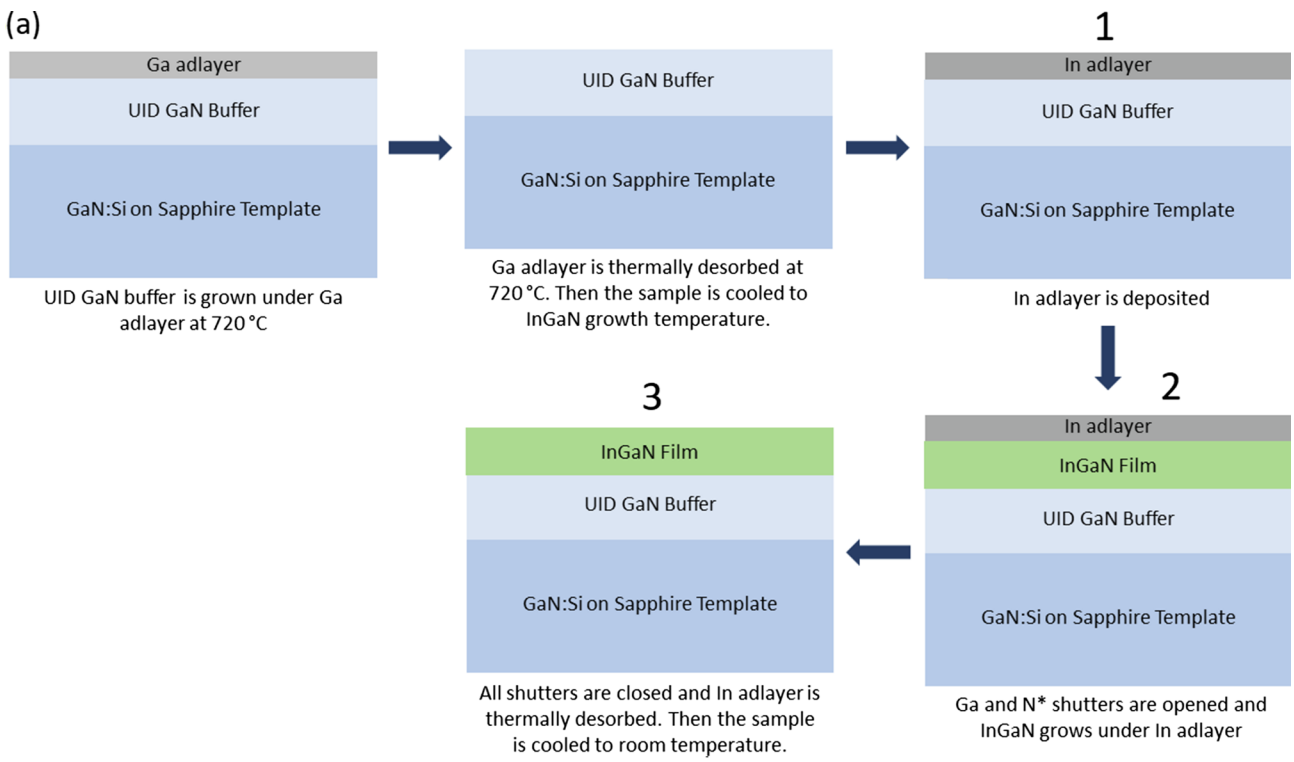


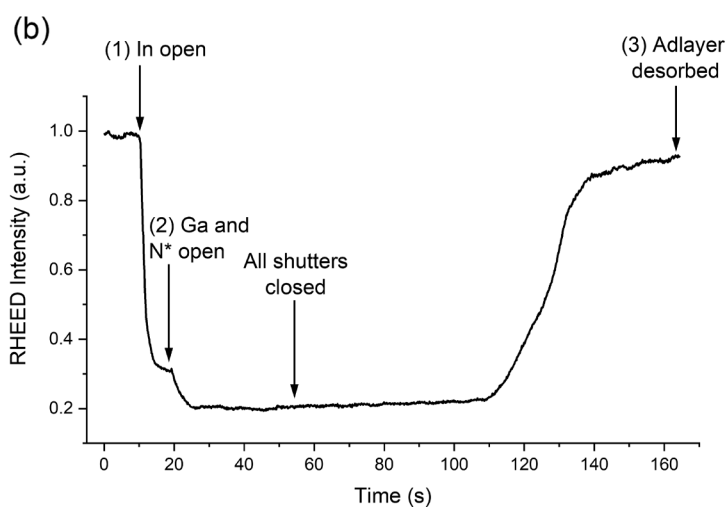


**Fig. 1.** (a). Schematic for GaN buffer and $In_xGa_{1-x}N$ film growth. Fig. 1(b) RHEED intensity transient for $In_xGa_{1-x}N$ growth showing the In adlayer formation, growth of the film, and adlayer thermal desorption.

**Table 1**
Growth details for Series 2. Fluxes are noted in terms of GaN equivalent growth rates for Ga and N*, InN equivalent growth rates for In, as well as atomic fluxes.

| Sample | Growth Temperature (°C) | $\Phi_{In}$ (μm/h) (atom/cm$^2$ s) | $\Phi_{N*}$ (μm/h) (atom/cm$^2$ s) | $\Phi_{N*}$-$\Phi_{Ga}$ (μm/h) (atom/cm$^2$ s) | $In_xGa_{1-x}N$ Composition x | $In_xGa_{1-x}N$ Growth Rate (μm/h) |
|---|---|---|---|---|---|---|
| A2 | 650 | 1.89<br>*2.31 × 10$^{15}$* | 2.6<br>*3.2 × 10$^{15}$* | 2.50<br>*3.05 × 10$^{15}$* | 0.148[a] | 0.14[a] |
| B2 | 650 | 3.17<br>*3.87 × 10$^{15}$* | 2.6<br>*3.2 × 10$^{15}$* | 2.50<br>*3.05 × 10$^{15}$* | 0.177[a] | 0.15[a] |
| C2 | 700 | 3.70<br>*4.52 × 10$^{15}$* | 3.5<br>*4.3 × 10$^{15}$* | 1.57<br>*1.92 × 10$^{15}$* | 0.05[b] | 0.06[b] |

[a] Values from HRXRD.
[b] Values from APT.

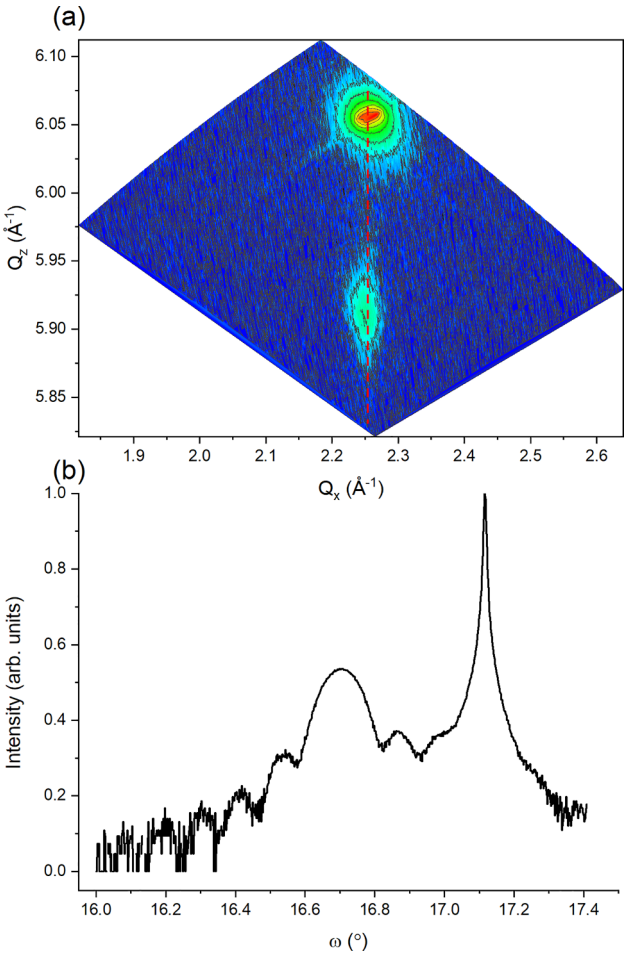


**Fig. 2.** (a). RSM of the $(10\bar{1}5)$ peak of a representative sample from Series 1 of composition $In_{0.15}Ga_{0.85}$ grown at 600 °C. The vertical dashed line is a guide to the eye showing that the film is coherent to the GaN substrate. Fig. 2(b) HRXRD ω-2θ triple axis scan of the (0002) peak of the same sample in 2(a). The peak separation between the GaN substrate peak and $In_xGa_{1-x}N$ alloy peak was used to calculate the alloy composition for all samples. The spacing between the smaller fringes was used to calculate the $In_xGa_{1-x}N$ thickness and growth rate.

($4.3 \times 10^{15}$ atom/cm$^2$s), the $N_2$ flow rate was 15 sccm, and a plasma forward power of 500 W was used. Due to the higher growth temperature used for Series 2, the $In_xGa_{1-x}N$ was capped with a thin (5 nm) GaN layer to prevent $In_xGa_{1-x}N$ decomposition during cooling. To grow the cap layer a second Ga cell with a flux larger than $\Phi_{N^*}$ was opened while the Ga cell used for $In_xGa_{1-x}N$ growth was closed. The In cell was left open. Using $\Phi_{Ga} > \Phi_{N^*}$ should prevent any In from incorporating into the cap layer.

At the end of growth for all samples, all cells were shuttered at the same time and the metal adlayer was desorbed as indicated by the RHEED intensity. Once the cells were shuttered, the intensity of the RHEED pattern first increased and then reached a constant steady state value consistent with a fully desorbed adlayer. Then the samples were cooled quickly to prevent $In_xGa_{1-x}N$ decomposition. The RHEED pattern of the final $In_xGa_{1-x}N$ films ranged from spotty (indicating a 3D surface) for the low $\Phi_{In}$ films to streaky (indicating a 2D surface) for the higher $\Phi_{In}$ films.

For each $In_xGa_{1-x}N$ film high resolution x-ray diffraction (HRXRD) ω-2θ scans of the 0002 reflection were recorded using a Philips Panalytical MRD Pro system with CuKα$_1$ radiation with a 4-bounce Ge (220) monochromator and 2-bounce Ge (220) analyzer. Reciprocal space maps (RSMs) of the $(1\ 0\ \bar{1}\ 5)$ reflection were collected using a PIXcel$^{3D}$ detector to confirm that the $In_xGa_{1-x}N$ films were fully coherent with the GaN substrate. $In_xGa_{1-x}N$ film thickness was determined by the spacing of the fringes of the ω-2θ 0002 scan.

The peak separation between the GaN and $In_xGa_{1-x}N$ (0002) peaks was used to determine the $In_xGa_{1-x}N$ alloy composition. Reference values used for the relaxed lattice parameters for pure GaN were $a_0$ = 3.1896 Å and $c_0$ = 5.1855 Å [15]. Reference values used for the relaxed lattice parameters for InN were $a_0$ = 3.5378 Å and $c_0$ = 5.7033 Å [16]. Reference values used for the elastic stiffness tensor elements $C_{13}$ and $C_{33}$ for pure wurtzite GaN and InN were taken from Ref. [17]. The wavelength for the CuKα$_1$ radiation was 1.5406 Å. The procedure to determine the $In_xGa_{1-x}N$ composition is as follows and is based on the assumption that the $In_xGa_{1-x}N$ film is fully coherent to the GaN substrate. First the measured GaN-$In_xGa_{1-x}N$ peak separation and the GaN relaxed reference $c_0$ lattice parameter were substituted into Bragg's law to determine the measured c lattice spacing of the $In_xGa_{1-x}N$ film. Then a starting guess for alloy composition was chosen. Vegard's law was used to determine the relaxed c and a lattice spacings for $In_xGa_{1-x}N$ as a function of composition from pure GaN and pure InN. Vegard's law was also used to determine the values of $C_{13}$ and $C_{33}$ for $In_xGa_{1-x}N$ as a function of composition based on the values for pure GaN and InN. Then the relaxed $In_xGa_{1-x}N$ a lattice parameter was used to calculate the in-plane strain ($\varepsilon_{||}$) via $\epsilon_{||} = \frac{a_{InGaN}}{a_{InGaN,relaxed}} - 1$. The measured a lattice spacing of the film is known since all $In_xGa_{1-x}N$ films grown were fully strained to the GaN substrate. The relationship between $\varepsilon_{||}$ and the out-of-plane strain ($\varepsilon_{\perp}$) is $\epsilon_{\perp} = -2\frac{C_{13}}{C_{33}}\epsilon_{||}$. The c lattice parameter calculated from $\varepsilon_{\perp}$ is $c_{InGaN} = c_{InGaN,measured} - (c_{0,GaN} \times \epsilon_{\perp})$. This c lattice parameter is then compared to the value obtained from Vegard's law. If the two values do not match, a new guess composition was chosen. This iterative process is performed by MATLAB until the two values match.

The ω-2θ 0002 scans were also used to determine whether In droplets were present on the surface of the $In_xGa_{1-x}N$ films. It has been documented that an In metal body-centered tetragonal (101) peak exists at an ω value approximately 0.8° less than that of the GaN (0002) substrate peak [18,19].

The surface morphology of each film was characterized via atomic force microscopy (AFM) using an Asylum MFP-3D tool used in the tapping mode in air. Scans were taken at 20 × 20, 5 × 5, and 1 × 1 μm. Root mean squared (RMS) roughness values are reported for 5 × 5 μm scans.

Sample C2 of Series 2 was also characterized via atom probe tomography (APT) to determine the alloy composition of the film [20]. The sample was cleaved and a 150 nm sacrificial GaN capping layer was grown at 720 °C under standard Ga-rich conditions sample to facilitate the preparation of the APT sharp tip. A FEI Helios 600 dual beam FIB instrument was used for the preparation of the specimen [21]. APT experiments were performed with a Cameca 3000X HR Local Electrode Atom Probe (LEAP) operated in laser-pulse mode (13 ps pulse, 532 nm green laser, 10 μm laser spot size) with a sample based temperature of 45 K. The laser pulse energy and the detection rate for the experiments were respectively set to 0.5 nJ and 0.02 atoms per pulse. The 3D reconstruction were carried out using a geometrical based algorithm [22] implemented in the commercial software IVAS$^{TM}$.

## 3. Results

### 3.1. Series 1

Fig. 2(a) and (b) show representative RSM and ω-2θ scans of a sample from Series 1 of composition $In_{0.15}Ga_{0.85}N$ grown at 600 °C. Since all films were fully coherent, the $In_xGa_{1-x}N$ composition was determined from 0002 ω-2θ scans. Not all films had well-defined thickness fringes to accurately determine the $In_xGa_{1-x}N$ thickness. However, among the samples that did have assessable thickness fringes, the $In_xGa_{1-x}N$ growth rates were consistently around 1.2 μm/h, with the highest growth rate measured of 1.3 μm/h. No identifiable trend was

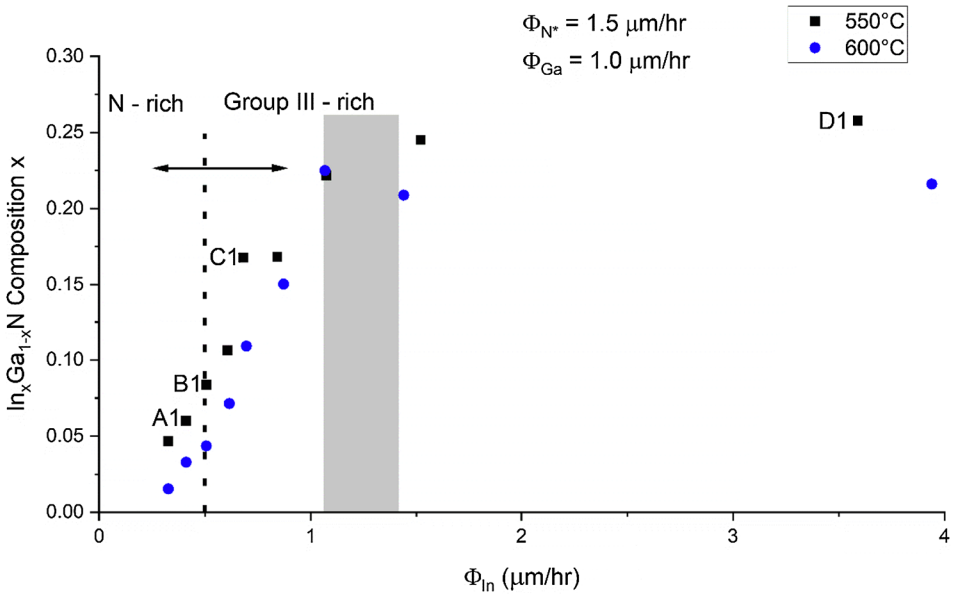


**Fig. 3.** $In_xGa_{1-x}N$ film composition x of Series 1 as a function of $\Phi_{In}$ and growth temperature. Alloy compositions increases linearly with $\Phi_{In}$ for each growth temperature until a saturated In wetting layer is reached. The gray region represents when the In wetting layer becomes saturated. The dashed line indicates the transition from N-rich growth to group III-rich growth.

observed in the growth rate as $\Phi_{In}$ was increased.

Fig. 3 shows the dependence of composition on $\Phi_{In}$ for all 14 samples of Series 1. As expected, alloy composition increases linearly with $\Phi_{In}$ until a saturated In wetting layer was realized. Once a saturated In wetting layer had formed, the film composition no longer changed with increasing $\Phi_{In}$. Films grown in the saturated In wetting layer regime all showed an In metal (101) peak in the ω-2θ 0002 scan, indicating that a saturated wetting layer was reached for both growth temperatures. The $\Phi_{In}$ required to reach a saturated wetting layer was 1.07 µm/h (1.31 × $10^{15}$ atom/cm$^2$s) for a growth temperature of 550 °C and 1.44 µm/h (1.31 × $10^{15}$ atom/cm$^2$s) for a growth temperature of 600 °C. The dashed line in Fig. 3 indicates the transition from N-rich growth to group III-rich growth. Due to desorption of In from the surface of the sample the $\Phi_{In}$ required to achieve a saturated In wetting layer is greater than that required to push the growth into the metal-rich regime. HRXRD ω-2θ 0002 scans of all seven samples grown at 600 °C is shown in Fig. 4. The In droplet (101) peak is visible for the two scans with highest $\Phi_{In}$. The saturated In composition was x = 0.25 for samples grown at 550 °C and x = 0.21 for samples grown at 600 °C.

Four representative samples (A1, B1, C1, and D1) from Series 1 are identified on Fig. 3. AFM scans of these samples are shown in Fig. 5. Samples A1 and B1 show mound-type structures forming around threading dislocations, which is similar to the spiral hillock formation reported in other studies of $In_xGa_{1-x}N$ grown by PAMBE [23]. Samples C1 and D1 do not have clear mound structures. AFM scans are shown on these samples because their morphologies are representative of the other samples in Series 1. The RMS roughness values calculated for samples A1, B1, C1, and D1 are 1.05 nm, 0.93 nm, 1.04 nm, and 1.79 nm, respectively.

### 3.2. Series 2

Once the high $\Phi_{N*}$ $In_xGa_{1-x}N$ growth was established at lower temperatures in Series 1, higher $\Phi_{N*}$ was used to determine how hot $In_xGa_{1-x}N$ could be grown with sufficient In incorporation. Table 1 shows the alloy compositions achieved for samples grown at 650 °C and 700 °C. The alloy composition for samples A2 and B2 were determined via HRXRD in the same way as samples in Series 1. At a growth temperature of 650 °C an alloy composition of x = 0.148 was achieved for sample A2 with $\Phi_{In}$ = 1.89 µm/h (2.31 × $10^{15}$ atom/cm$^2$s) and x = 0.177 was achieved for sample B2 with $\Phi_{In}$ = 3.17 µm/h (3.87 × $10^{15}$ atom/cm$^2$s). A saturated In wetting layer was not observed for any of the samples in Series 2. AFM scans for samples A2 and B2 show a mound morphology similar to samples A1 and B1 in Series 1 and have RMS roughness values of 1.40 nm and 1.61 nm respectively.

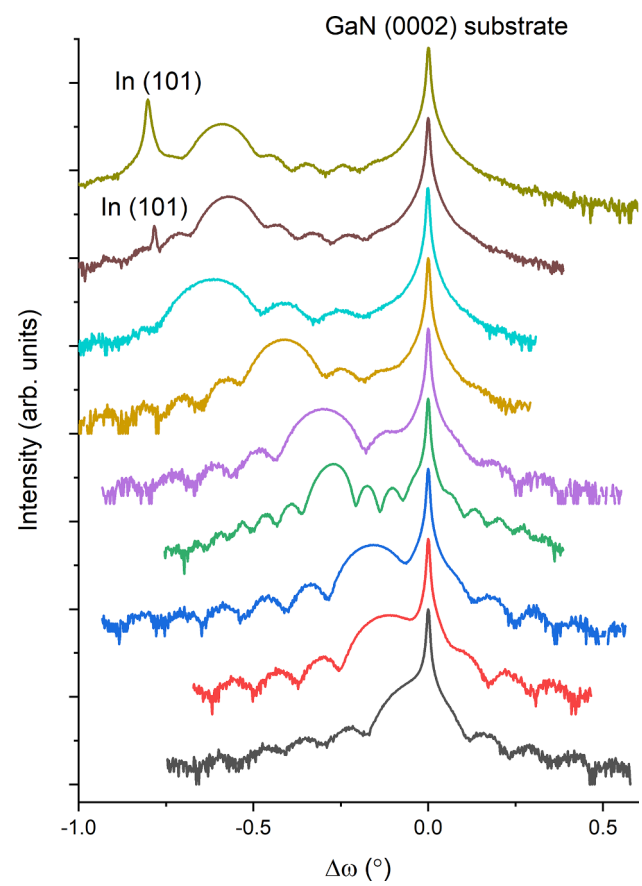


**Fig. 4.** HRXRD ω-2θ scans of all samples in Series 1 grown at 600 °C. Δω refers to the distance in degrees from the GaN (0002) substrate peak. The $In_xGa_{1-x}N$ alloy peaks are at a smaller ω than the GaN substrate peak.

Determination of the film composition for sample C2 grown at 700 °C was not possible via HRXRD. The ω-2θ 0002 scan for sample C2 (shown in Fig. 6) did not have a separate alloy peak. Thickness fringes are visible, but it is unclear if they are from the GaN cap layer or an $In_xGa_{1-x}N$ layer. The APT 3D reconstruction of sample C2 shown in

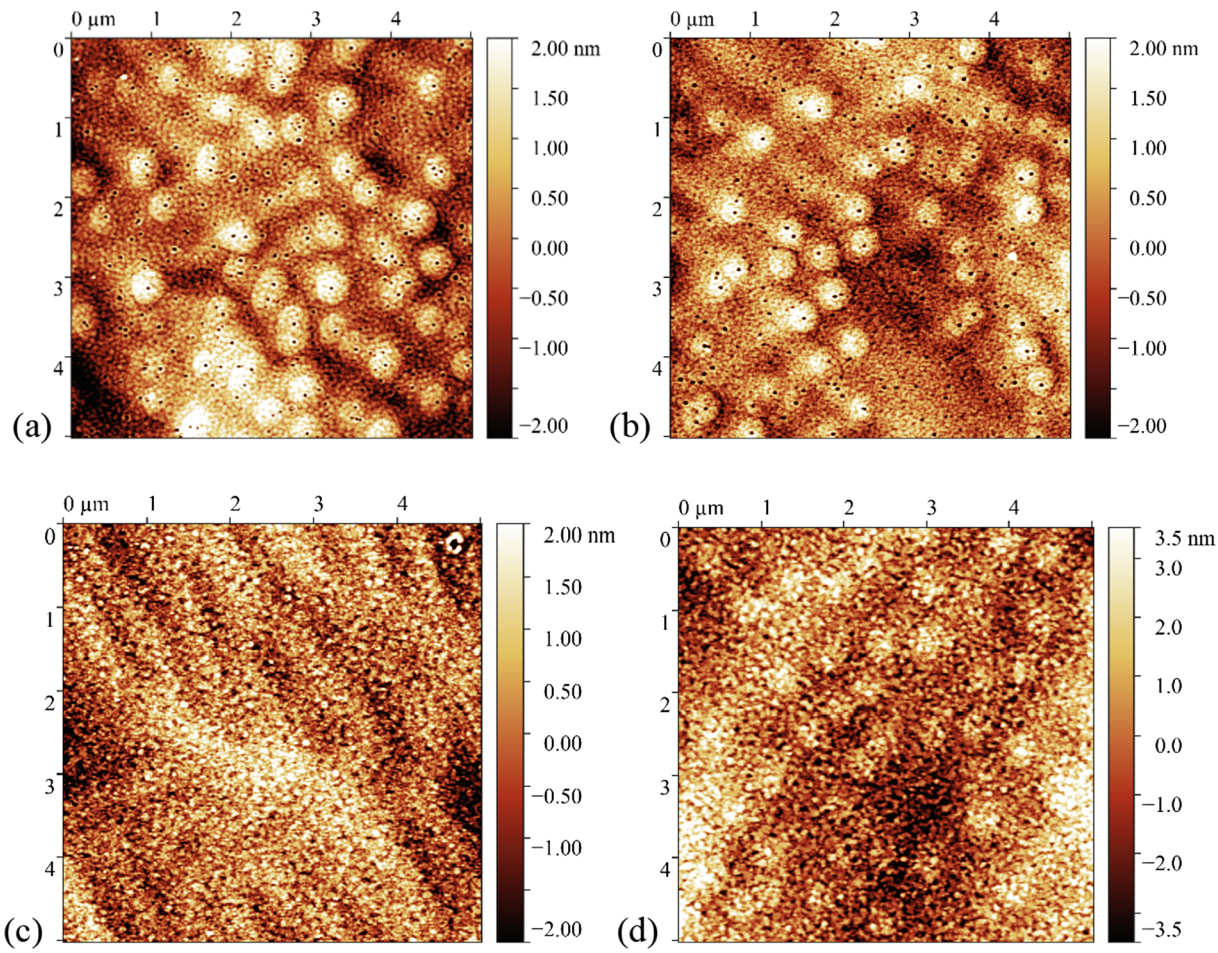


**Fig. 5.** 5 × 5 µm AFM scans from samples (a) A1, (b) B1, (c) C1, and (d) D1 in Series 1. RMS roughness values are 1.05 nm, 0.93 nm, 1.04 nm, and 1.79 nm, respectively.

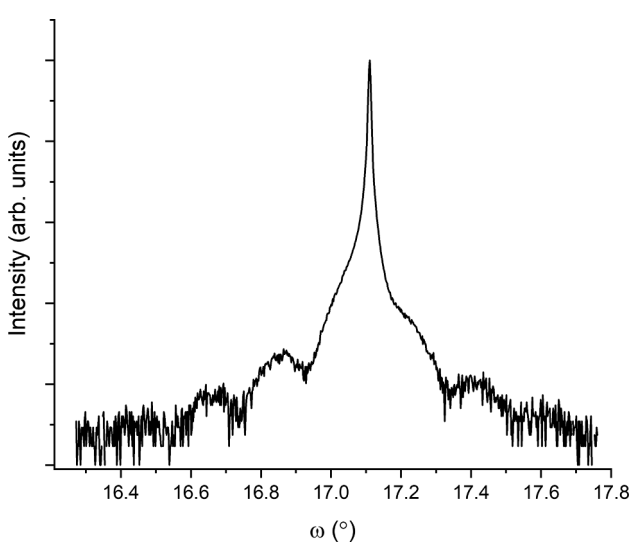


**Fig. 6.** HRXRD ω-2θ scan of sample C2 from Series 2 showing thickness fringes, but no separate $In_xGa_{1-x}N$ alloy peak.

Fig. 7(a) and the corresponding In 1D concentration profile along the growth direction in Fig. 7(b) indicates an $In_xGa_{1-x}N$ composition of x = 0.05. The film thickness was less than 10 nm, resulting in a growth rate of only 1–2 nm/min.

In the 1D concentration profile in Fig. 7(b) Sample C2 also shows around x = 0.005 In incorporation in the GaN cap layer. Since the In source shutter was open during the GaN cap growth, it is possible that the In incorporated as the film was grown even though $\Phi_{Ga}$ was greater than $\Phi_{N^*}$, which should prevent any In incorporation.

The 5 × 5 µm AFM scan of sample C2 is shown in Fig. 8. This samples does not show mound morphology, but rather step-terrace morphology and has an RMS roughness of 0.70 nm. It is important to note that the morphology could be in part attributed to the thin (5 nm) GaN cap rather than the underlying $In_xGa_{1-x}N$.

## 4. Discussion

As shown in Fig. 3, once a saturated In wetting layer is reached, the film composition no longer changes with increasing $\Phi_{In}$. This is the first confirmation that PAMBE $In_xGa_{1-x}N$ growth at high growth rates follows the same trend with increasing $\Phi_{In}$ as observed at the more common growth rates around 200 – 300 nm/h [18,19]. Hestroffer et al. [19] reported a saturated In composition of x = 0.18 for a growth temperature of 575 °C and Gacevic et al. [18] reported In compositions ranging from x = 0 to x = 0.50 depending on growth temperature and incident $\Phi_{In}$.

Even though there is no thermodynamic equilibrium during MBE growth (since it is impossible to define a temperature for the molecular beam), the saturation of the In content in the films can be understood as the chemical potential of In in the film ($\mu_{In,\ film}$) being equal to the chemical potential of liquid In in the droplets and wetting layer ($\mu_{In,\ drop}$). So $\mu_{In,\ wetting\ layer} = \mu_{In,\ droplet} = \mu_{In,\ film}$. The In droplets act as an In reservoir that "feeds" the adlayer. A schematic representing the In exchange is shown in Fig. 9.

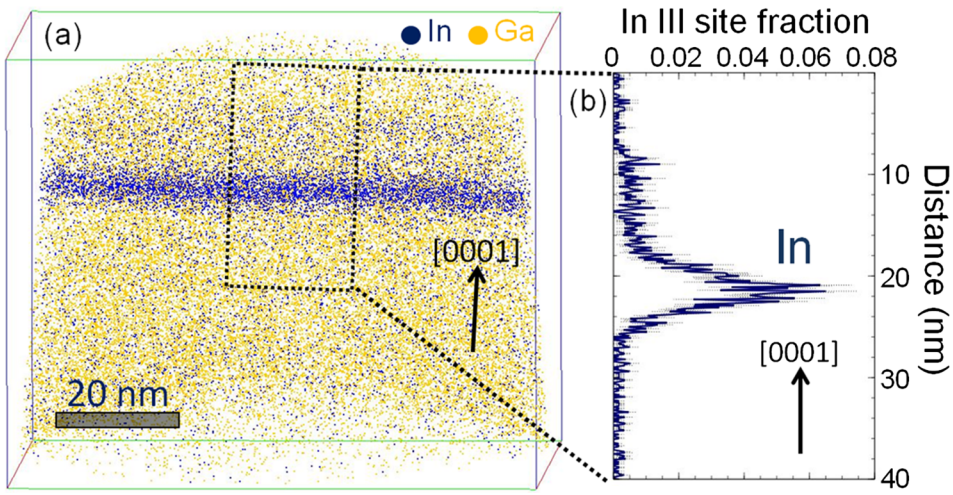


**Fig. 7.** (a). APT 3D reconstruction of sample C2 in Series 2 shown an $In_xGa_{1-x}N$ layer is present. Fig. 7(b). 1D concentration profile measured from the center of the 3D reconstruction and along the growth direction showing the amount of In incorporated in the layer and above it.

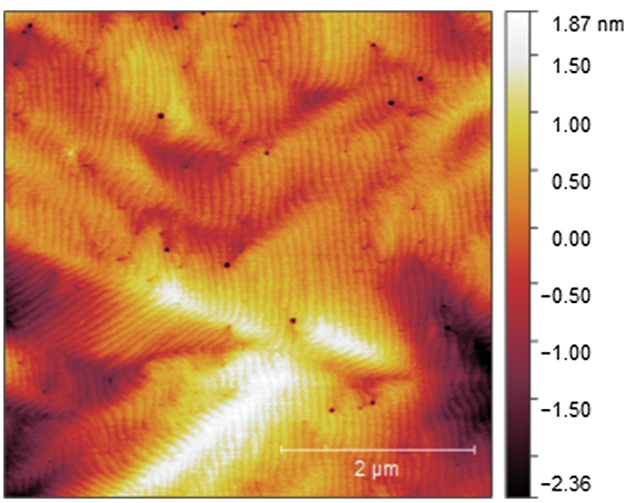


**Fig. 8.** AFM scan of sample C2 from Series 2 showing step-terrace surface morphology and a RMS surface roughness of 0.70 nm.

It is also clear that there is a large desorbing $\Phi_{In}$ from the sample surface during $In_xGa_{1-x}N$ growth from desorption of In from the adlayer. Note in these studies $\Phi_{In} + \Phi_{Ga} > \Phi_{N^*}$ for most samples and thus we expect at steady state there must be significant In desorption as Ga should preferentially incorporate over In in the growing $In_xGa_{1-x}N$ film for metal-rich growth. A comparison of the vapor pressure of liquid In and Ga at relevant growth temperatures illustrates this desorbing $\Phi_{In}$. At a growth temperature of 600 °C, $p_{In,\ liq} = 1.6\times10^{-6}$ Torr and $p_{Ga,\ liq} = 4.1\times10^{-8}$ Torr [24]. Almost two orders of magnitude difference in vapor pressure results in a film that has a much lower In content than would be expected based on the ratio of $\Phi_{In}/\Phi_{Ga}$ alone. This $p_{In,\ liq}$ is approximately equal to the BEP of In. At the even higher growth temperatures explored in Series 2 (650 °C and 700 °C), the difference in vapor pressures between the two group III elements is even larger. At 700 °C there is 3 orders of magnitude difference between $p_{In,\ liq}$ and $p_{Ga,\ liq}$. Once the In wetting layer is saturated, the equilibrium desorbing In flux is equal to the vapor pressure of In, $\Phi_{In,\ desorb} = \Phi_{In,\ liq}$.

This large desorbing $\Phi_{In}$ becomes more extreme as growth temperature increases. At 700 °C the net $In_xGa_{1-x}N$ growth rate is so low that the film is barely growing faster than it is decomposing. For growth temperatures of 650 °C and below, the growth rate is governed mainly by $\Phi_{Ga}$ forming Ga-N bonds, with a small component being added from the In that actually participates in bonding. For sample C2 the growth rate does not follow $\Phi_{Ga}$ = 1.03 µm/h, which suggests Ga-N bonds are also decomposing.

For growth with a saturated In wetting layer, the film composition is determined by the growth temperature and the $\Phi_{N^*}$ - $\Phi_{Ga}$ deficit. It seems that growth temperature has a larger effect than the absolute $\Phi_{N^*}$, although this work does not include samples grown at the more common $\Phi_{N^*}$ 0.2 – 0.3 µm/h for comparison. The formation of the saturated In wetting layer represents the maximum chemical potential for In ($\mu_{In,\ max}$) for a given growth temperature and $\Phi_{N^*}$ - $\Phi_{Ga}$ deficit. Thus the maximum In incorporation under a saturated In wetting layer

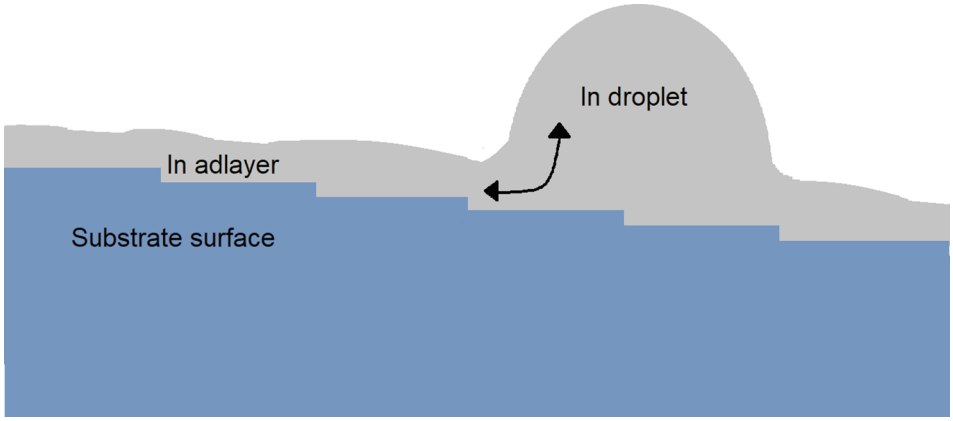


**Fig. 9.** Schematic showing In exchange between the droplets and In adlayer present on the growing film.

represents the solubility limit of In in $In_xGa_{1-x}N$ for that growth temperature and $\Phi_{N^*}$-$\Phi_{Ga}$ deficit.

In Ref. [19], which reports a maximum growth rate of 265 nm/h under a saturated In wetting layer, the growth rate is shown to increase linearly from 200 nm/h to 260 nm/h with increasing $\Phi_{In}$ just like film composition. This is not observed for high growth rate $In_xGa_{1-x}N$ in this work. This is because the overall growth rate is so high that the small incremental change provided by slightly more In incorporation is not large enough to be more than noise.

Samples A1, B1, A2, and B2 all exhibit mound morphology. But as $\Phi_{In}$ increases and the growth temperature increases, samples exhibit planar morphology, with atomic steps visible on sample C2 but not on samples C1 and D1. This indicates that as the In adlayer develops and the growth temperature increases, surface adatom mobility is enhanced, thus eliminating the mound structures.

Since the motivation for growing $In_xGa_{1-x}N$ at high active nitrogen fluxes was derived in part from extrapolating the modeling by Turski et al. [6], it is important to see if the present work follows the trends seen in that work conducted at lower growth rates. Previous models for PAMBE growth of $In_xGa_{1-x}N$ expressed the desorbing nitrogen flux ($\Phi_N^{\nearrow}$) due to In-N bond decomposition as $\Phi_N^{\nearrow} = C \bullet x \bullet exp\left(-\frac{E_a(x)}{kT}\right)$ where C is a constant, x is the film composition, $E_a$ is an energy barrier that depends on film composition x, and T is the growth temperature [25]. In Ref. [6] however, the authors point out that on a vicinal GaN surface there are two types of c/2 atomic steps (A and B) that differ in the number of bonds a N atom landing on the surface can satisfy. Based on these "non-equivalent" atomic steps they express the desorbing nitrogen flux as $\Phi_N^{\nearrow} = \left(\frac{C_A}{\Phi_N^{\searrow}} + \frac{C_B}{\Phi_{Ga}^{\searrow}}\right) \bullet (\Phi_N^{\searrow} - \Phi_{Ga}^{\searrow}) \bullet exp\left(-\frac{E_a(x)}{kT}\right)$ where $C_A$ and $C_B$ are constants associated with atomic steps A and B, respectively and $\Phi_N^{\searrow}$ and $\Phi_{Ga}^{\searrow}$ are the incident N and Ga fluxes, respectively. Then the study goes on to grow a series of $In_xGa_{1-x}N$ films at a variety of different $\Phi_{N^*}$, $\Phi_{Ga}$, and growth temperatures to fit the constants $C_A$ and $C_B$. It is important to note that in Ref. [6] the authors state that all samples were grown under a saturated In wetting layer.

If the nonequivalent atomic step model presented in Ref. [6] is extrapolated to the growth rates in Series 1 of this work, the maximum In incorporation at a growth temperature of 550 °C and 600 °C is predicted to be 32.4% and 28.4%, respectively. This is higher than the observed maximum In incorporation of 25.8% and 22.5%. This could be due to differences in growth temperature between different MBE systems (since optical pyrometry is only a precise, but not necessarily accurate technique). Since the maximum $\Phi_{N^*}$ used by Turski et. al [6] is 0.55 μm/h ($6.72 \times 10^{15}$ atom/cm$^2$s), it could also be the case that extrapolating to $\Phi_{N^*}$ = 1.0 μm/h ($1.2 \times 10^{15}$ atom/cm$^2$s) is beyond the limits of the model's accuracy. It is important to note that since the modeling assumes the presence of a saturated In wetting layer, it is not appropriate to apply the model to Series 2, where all samples are grown before the onset of a saturated In wetting layer.

Since impurity incorporation in growing films is inversely proportional to the growth rate, growing $In_xGa_{1-x}N$ films at these elevated growth rates could greatly improve the material quality and could lead to more efficient PAMBE III-N LEDs. One important consideration in the growth of $In_xGa_{1-x}N$/GaN active regions is having precise control over the thickness of quantum wells. Growth rates that are too high could lead to a loss of control over film thickness if the growth time approaches the MBE shutter rise and fall times. Even at the highest growth rate reported in this work (1.3 μm/h), a 3 nm quantum well corresponds to a 8.4 s growth time, which is sufficiently longer than the approximately 5 ms shutter rise and fall time. Elevated growth rates could also be useful for growing thick, relaxed $In_xGa_{1-x}N$ layers for applications where strain reduction of higher In composition layers is desirable.

Future work is currently planned to determine the maximum possible In content in $In_xGa_{1-x}N$ films at 700 °C. While it may be possible through optimization of growth conditions to reach film compositions useful for blue emitting optoelectronic devices, it seems unlikely that higher compositions corresponding to longer wavelength devices is possible at such high growth temperatures.

Growth at these elevated atomic fluxes comes with logistical challenges, however. Several modifications have been made to the MBE system in this study over the years that this high flux plasma unit has been in use. When group III effusion cells are operated at high capacity for an extended length of time, source material can be depleted rapidly. Over the history of high-flux research at our university, both Ga effusion cells and the In effusion cell have been replaced with higher capacity cells to reduce downtime related to source material refilling. With $N_2$ gas flows as high as 15 sccm, extra pumping has been added to the system to keep the pressure during growth at an acceptable level. During high flux growth, it is typical for the growth chamber pressure to reach the mid $10^{-5}$ Torr range. Parts inside the chamber can become coated in III-N material quickly, requiring more frequent replacement and cleaning of parts like mounting blocks, RHEED screens, and viewports. The extra cost associated with these issues may prove to be unrealistic for some groups.

Another technical consideration is that the high-flux plasma unit is currently not capable of growing at the more traditional lower growth rates (around 300 nm/h) on which earlier work from our group was based. Instead of replacing the older plasma unit, we have opted to keep both the lower-flux and higher-flux units on the system. This uses an extra source port that some MBE systems might not have to spare. As more work on the possibilities of high-flux PAMBE III-N growth is done, groups will have to weigh the benefits and costs of this new technique.

## 5. Conclusion

In this work we investigated the effect of high active nitrogen flux on the incorporation of In into $In_xGa_{1-x}N$ films at low and elevated growth temperatures. Using a high $\Phi_{N^*}$ at lower PAMBE $In_xGa_{1-x}N$ growth temperatures resulted in record high $In_xGa_{1-x}N$ growth rates of up to 1.3 μm/h and mound-like surface morphology. In incorporation follows linearly with $\Phi_{In}$ before the onset of a saturated In wetting layer, just as for lower growth rate $In_xGa_{1-x}N$ reported in the literature.

We have also shown that In incorporation into $In_xGa_{1-x}N$ films is possible at 700 °C, which has not been demonstrated previously in the literature. The film grown at 700 °C shows very smooth step-terrace surface morphology and no spiral hillocks. It is expected that increasing $\Phi_{N^*}$ further will result in more In incorporation. It is important to note that at 700 °C the $In_xGa_{1-x}N$ growth rate is only a few nm/min even though the constituent fluxes are all over 1.0 μm/h ($1.2 \times 10^{15}$ atom/cm$^2$s). This is because the film is decomposing so quickly that the net growth rate is extremely slow.

Further optimization of $In_xGa_{1-x}N$ at 700 °C is planned to maximize In incorporation into the film. Optical characterization of $In_xGa_{1-x}N$ films grown with high $\Phi_{N^*}$ is also planned as well as eventual integration into all PAMBE LEDs. This work represents an viable path forward to achieving efficient III-N PAMBE LEDs.

## CRediT authorship contribution statement

**Kelsey F. Jorgensen:** Conceptualization, Methodology, Formal analysis, Investigation, Writing - original draft, Writing - review & editing, Visualization. **Bastien Bonef:** Formal analysis, Writing - original draft, Writing - review & editing, Visualization. **James S. Speck:** Conceptualization, Methodology, Resources, Writing - review & editing, Supervision, Project administration, Funding acquisition.

## Declaration of Competing Interest

The authors declare that they have no known competing financial

interests or personal relationships that could have appeared to influence the work reported in this paper.

## Acknowledgements

This work was supported in part by the KACST-KAUST-UCSB Solid State Lighting Program, the Solid State Lighting and Energy Electronics Center (SSLEEC) at UCSB, the Simons Foundation (601952, JS), and (NSF) RAISE program (Grant No. A007231601, JS).

## References

[1] C.S. Gallinat, G. Koblmuller, J.S. Brown, J.S. Speck, A growth diagram for plasma-assisted molecular beam epitaxy of In-face InN, J Appl Phys. 102 (2007) 064907, , https://doi.org/10.1063/1.2781319.

[2] M.J. Grundmann, U.K. Mishra, Multi-color light emitting diode using polarization-induced tunnel junctions, Phys. Status Solidi (c) 4 (2007) 2830–2833, https://doi.org/10.1002/pssc.200675000.

[3] C. Skierbiszewski, Z.R. Wasilewski, I. Grzegory, S. Porowski, Nitride-based laser diodes by plasma-assisted MBE-From violet to green emission, J Cryst Growth. 311 (2009) 1632–1639, https://doi.org/10.1016/j.jcrysgro.2008.12.040.

[4] P. Waltereit, H. Sato, C. Poblenz, D.S. Green, J.S. Brown, M. McLaurin, T. Katona, S.P. DenBaars, J.S. Speck, J.-H. Liang, M. Kato, H. Tamura, S. Omori, C. Funaoka, Blue GaN-based light-emitting diodes grown by molecular-beam epitaxy with external quantum efficiency greater than 1.5%, Appl. Phys. Lett. 84 (2004) 2748–2750, https://doi.org/10.1063/1.1705721.

[5] S. Fernandez-Garrido, G. Koblmuller, E. Calleja, J.S. Speck, In situ GaN decomposition analysis by quadrupole mass spectrometry and reflection high-energy electron diffraction, J. Appl. Phys. 104 (2008) 033541, , https://doi.org/10.1063/1.2968442.

[6] H. Turski, M. Siekacz, Z.R. Wasilewski, M. Sawicka, S. Porowski, C. Skierbiszewski, Nonequivalent atomic step edges-Role of gallium and nitrogen atoms in the growth of InGaN layers, J. Cryst. Growth. 367 (2013) 115–121, https://doi.org/10.1016/j.jcrysgro.2012.12.026.

[7] J. Osaka, M. Senthil Kumar, H. Toyoda, T. Ishijima, H. Sugai, T. Mizutani, Role of atomic nitrogen during GaN growth by plasma-assisted molecular beam epitaxy revealed by appearance mass spectrometry, Appl. Phys. Lett. 90 (2007) 172114, , https://doi.org/10.1063/1.2734390.

[8] K. Klosek, M. Sobanska, G. Tchutchulashvili, Z.R. Zytkiewicz, H. Teisseyre, L. Klopotowski, Optimization of nitrogen plasma source parameters by measurements of emitted light intensity for growth of GaN by molecular beam epitaxy, Thin Solid Films. 534 (2013) 107–110, https://doi.org/10.1016/j.tsf.2013.02.013.

[9] E. Iliopoulos, A. Adikimenakis, E. Dimakis, K. Tsagaraki, G. Konstantinidis, A. Georgakilas, Active nitrogen species dependence on radiofrequency plasma source operating parameters and their role in GaN growth, J. Cryst. Growth. 278 (2005) 426–430, https://doi.org/10.1016/j.jcrysgro.2005.01.013.

[10] M. Siekacz, A. Feduniewicz-Żmuda, G. Cywiński, M. Kryśko, I. Grzegory, S. Krukowski, K.E. Waldrip, W. Jantsch, Z.R. Wasilewski, S. Porowski, C. Skierbiszewski, Growth of InGaN and InGaN/InGaN quantum wells by plasma-assisted molecular beam epitaxy, J. Cryst. Growth. 310 (2008) 3983–3986, https://doi.org/10.1016/j.jcrysgro.2008.06.011.

[11] H. Turski, M. Siekacz, M. Sawicka, Z.R. Wasilewski, S. Porowski, C. Skierbiszewski, Role of Nonequivalent Atomic Step Edges in the Growth of InGaN by Plasma-Assisted Molecular Beam Epitaxy, Jpn. J. Appl. Phys. 52 (2013) 08JE02, https://doi.org/10.7567/JJAP.52.08JE02.

[12] B.M. McSkimming, C. Chaix, J.S. Speck, High active nitrogen flux growth of GaN by plasma assisted molecular beam epitaxy, J. Vac. Sci. Technol. A: Vac., Surf., Films. 33 (2015) 05E128, https://doi.org/10.1116/1.4928415.

[13] B.P. Gunning, E.A. Clinton, J.J. Merola, A. Doolittle, R.C. Bresnahan, Control of ion content and nitrogen species using a mixed chemistry plasma for GaN grown at extremely high growth rates >9 μm/h by plasma-assisted molecular beam epitaxy, J. Appl. Phys. 118 (2015) 155302, , https://doi.org/10.1063/1.4933278.

[14] G. Koblmüller, J. Brown, R. Averbeck, H. Riechert, P. Pongratz, J.S. Speck, Continuous evolution of Ga adlayer coverages during plasma-assisted molecular-beam epitaxy of (0001) GaN, Appl. Phys. Lett. 86 (2005) 041908, , https://doi.org/10.1063/1.1853530.

[15] M. Yamaguchi, T. Yagi, T. Sota, T. Deguchi, K. Shimada, S. Nakamura, Brillouin scattering study of bulk GaN, J. Appl. Phys. 85 (1999) 8502–8504, https://doi.org/10.1063/1.370635.

[16] W. Paszkowicz, X-ray powder diffraction data for indium nitride, Powder Diffraction. 14 (1999) 258–260, https://doi.org/10.1017/S0885715600010630.

[17] A.F. Wright, Elastic properties of zinc-blende and wurtzite AlN GaN, and InN, J. Appl. Phys.. 82 (1997) 2833–2839, https://doi.org/10.1063/1.366114.

[18] Z. Gacevic, V.J. Gomez, N.G. Lepetit, P.E.D. Soto Rodriguez, A. Bengoechea, S. Fernandez-Garrido, R. Notzel, E. Calleja, A comprehensive diagram to grow (0001) InGaN alloys by molecular beam epitaxy, J. Cryst. Growth 364 (2013) 123–127, https://doi.org/10.1016/j.jcrysgro.2012.11.031.

[19] K. Hestroffer, F. Wu, H. Li, C. Lund, S. Keller, J.S. Speck, U.K. Mishra, Relaxed c -plane InGaN layers for the growth of strain-reduced InGaN quantum wells, Semicond. Sci. Technol. 30 (2015) 105015, , https://doi.org/10.1088/0268-1242/30/10/105015.

[20] B. Bonef, M. Catalano, C. Lund, S.P. Denbaars, S. Nakamura, U.K. Mishra, M.J. Kim, S. Keller, Indium segregation in N-polar InGaN quantum wells evidenced by energy dispersive X-ray spectroscopy and atom probe tomography, Appl. Phys. Lett. 110 (2017) 143101, , https://doi.org/10.1063/1.4979786.

[21] K. Thompson, D. Lawrence, D.J. Larson, J.D. Olson, T.F. Kelly, B. Gorman, In situ site-specific specimen preparation for atom probe tomography, Ultramicroscopy. 107 (2007) 131–139, https://doi.org/10.1016/j.ultramic.2006.06.008.

[22] F. Vurpillot, B. Gault, B.P. Geiser, D.J. Larson, Reconstructing atom probe data: A review, Ultramicroscopy. 132 (2013) 19–30, https://doi.org/10.1016/j.ultramic.2013.03.010.

[23] K. Hestroffer, C. Lund, H. Li, S. Keller, J.S. Speck, U.K. Mishra, Plasma-assisted molecular beam epitaxy growth diagram of InGaN on (0001)GaN for the optimized synthesis of InGaN compositional grades, Phys. Stat. Sol. (b) 253 (2016) 626–629, https://doi.org/10.1002/pssb.201552550.

[24] C.B. Alcock, V.P. Itkin, M.K. Horrigan, Vapour Pressure Equations for the Metallic Elements: 298–2500K, Can. Metall. Quart. 23 (1984) 309–313, https://doi.org/10.1179/cmq.1984.23.3.309.

[25] R. Averbeck, H. Riechert, Quantitative Model for the MBE-Growth of Ternary Nitrides, Physica Status Solidi (a). 176 (1999) 301–305, https://doi.org/10.1002/(SICI)1521-396X(199911)176:1<301::AID-PSSA301>3.0.CO;2-H.